Title	Infrared thermography of the fumarole area in the active crater of the Aso volcano, Japan, using a consumer digital camera
Author(s)	Furukawa, Yoshitsugu
Citation	Journal of Asian Earth Sciences (2010), 38(6): 283-288
Issue Date	2010-06-01
URL	http://hdl.handle.net/2433/128901
Right	© 2010 Elsevier Ltd
Type	Journal Article
Textversion	author

Infrared thermography of the fumarole area in the active crater of the Aso volcano, Japan, using a consumer digital camera

Yoshitsugu Furukawa*

Division of Earth and Planetary Sciences, Graduate School of Science, Kyoto University, Kyoto 606-8502, Japan

*Tel.: +81 75 753 3910; fax: +81 75 753 3717
E-mail address: furukawa.yoshitsugu.5r@kyoto-u.ac.jp

Abstract

Thermal information of volcanoes is crucial for understanding their magmatic activity. In active volcanoes, the fumarole temperature is measured in order to monitor the magmatic activity. In this study, a consumer digital camera has been used as an infrared thermometer in order to obtain the infrared images for a fumarole area in the active crater of the Aso volcano, Japan; the temperature of the fumaroles that are more than a few centimeters in diameter can be estimated from the recorded images. The aperture value and the exposure time of the digital camera can be optimized manually, and clear images can be obtained in a wider temperature range of fumaroles by using the digital camera than by the consumer camcorder used in the previous study. The spatial resolution can also be chosen by changing the lens. The sensor of the digital cameras is sensitive to the near-infrared wavelengths of light, and the temperature estimation by using light of these wavelengths is robust against disturbances such as atmospheric absorption. The temperature, size, and spatial distribution of the fumaroles estimated by using this thermometer are considered to be more reliable than those measured by the dedicated thermometer used in the Aso volcano and the consumer camcorder used in the previous study. The thermometer used in this study is handy and cost-effective. Moreover, it has better temperature and spatial resolutions for monitoring high-temperature volcanic activity.

Keyword: infrared thermography; fumarole; digital camera; active crater; Aso Volcano

Introduction

Volcanic eruptions give crucial information about the magmatic processes in volcanoes; however, these are very dangerous phenomena and are difficult to observe at a closer location. In active volcanoes, high-temperature volcanic gases arising from the magmas flow out from the active fumaroles between eruptions. The temperature of the surface fumaroles can provide important inferences about the magmatic and the hydrothermal systems under active volcanoes (Giberti et al., 1992; Martini, 1986; Stevenson, 1993; Taran et al., 1995). Higher magmatic activity is expected to cause a higher flux of volcanic gases to the surface, and an increase in the fumarole temperatures has often been observed prior to eruptions or during shallow magma intrusions (Menyailov et al., 1986). Measurements of the fumarole temperature have been carried out in several volcanoes for understanding magmatic processes and detecting the precursors of eruptions as well as other geophysical and geochemical observations (Connor et al., 1993; Menyailov et al., 1986).

Human activities could easily suffer severe damage from even small volcanic eruptions. It is necessary to predict small bursts such as the ejection of debris, particularly for volcanoes and the areas surrounding their active craters that are visited by many tourists. The detection of a small change in volcanic activity, which might be a precursor to small eruptions, is necessary to mitigate volcanic hazards. The temperature of fumaroles in the active crater could reflect a near-surface thermal state and might exhibit some precursors of the small bursts (Ripepe et al., 2002). In situ temperature measurements in active craters are difficult to operate, and remote sensing techniques have been used for the quantitative measurements. Satellite images have been used

for monitoring volcanic activity (Flynn et al., 2000; Ramsey and Dehn, 2004); however, the spatial resolution of these images is not sufficiently high to monitor the temperature of the fumaroles (Harris and Stevenson, 1997). We have constructed an infrared thermometer by using a consumer camcorder and measured the temperature of the fumaroles in the active crater of the Aso volcano in Japan, which is a popular site among tourists (Saito et al., 2005). This thermometer is a cost-effective; however, its spatial resolution is not sufficiently high to estimate the temperature of the small fumaroles in the active crater of the Aso volcano. In this study, a consumer digital camera has been used as a high spatial- and temperature-resolution thermometer, and the temperature measurement has been carried out in a fumarole area in the active crater of the Aso volcano, Japan.

Infrared thermography

The intensity of radiated energy is proportional to the fourth power of the absolute temperature which is known as the Stefan-Boltzmann's law. The temperature of an object can be estimated by measuring its radiation intensity. The spectral energy density of blackbody radiation B(λ) is given by the Planck's equation,

$$B(\lambda) = \frac{2hc^2}{\lambda^5} \frac{1}{e^{hc/\lambda kT} - 1},$$

where h, c, k, λ, and T are Planck's constant, the speed of light, Boltzmann's constant, wavelength, and temperature, respectively. The radiation energy spectra are shown in Fig. 1. The peak wavelength of the spectrum becomes shorter as the temperature of the object increases,

while the radiation intensity increases with the temperature. The radiation energy in a spectral range varies with temperature and is therefore used in the temperature estimations.

The total radiation detected at a light sensor, $R(\lambda)$, is expressed as follows, when the temperature of an object is very high as compared to that of the surroundings and when atmospheric effects such as absorption and scattering can be neglected:

$$R(\lambda) = \varepsilon_\lambda B(\lambda) + \rho_\lambda B_S(\lambda),$$

where ε_λ, ϱ_λ, and $B_s(\lambda)$ are the emissivity of the object, reflectance of the object, and solar radiation intensity at the surface, respectively. The second term on the right-hand side of the above equation is the reflected sunlight at the surface of the object, which is a disturbance in the temperature estimation. The emissivity of rocks depends primarily on their composition and the wavelengths of the incident light. The emissivity was estimated to be 0.935 for volcanic surfaces at the Stromboli volcano in the spectral range of 1.55 to 1.75 μm (Harris and Stevenson, 1997); the measured emissivity value for the rough surface of basalts is about 0.95 for the spectral range of 3 to 5 μm (Salisbury and D'Aria, 1994). In the ASTER spectral library, the reflectance of basaltic rocks is about 0.079 on average at the wavelength of 1.0 μm (Baldridge et al., 2008). In this study, the reflectance is expected to be about 0.05 as determined by using the Kirchoff's law ($\varrho_\lambda = 1 - \varepsilon_\lambda$) in volcanic areas with basaltic lavas for the near-infrared wavelengths.

For the temperature estimations in the daytime, the solar radiation intensity should be considerably lower than the radiation intensity of an object for the spectral range used in the temperature measurements. For an object with relatively low temperatures (<500ºC), the thermal infrared wavelengths of about 10 μm are generally used in the temperature measurements to

avoid the disturbance due to sunlight, while the near-infrared wavelengths from 1 to 2 μm are used for an object with relatively high temperatures (>500ºC) because the wavelength at the peak of the radiation intensity becomes much shorter than 10 μm and the solar radiation is negligible at the wavelengths (Fig. 1).

Radiation intensity is in the same order of magnitude for objects with the temperatures ranging from 300 to 1000ºC for the wavelength of 10 μm, while for the wavelength of 1 μm, the radiation intensity varies to six orders of magnitude for the objects within that temperature range. This indicates that the temperature estimation by using wavelengths of about 1 μm is expected to be robust against the disturbances affecting the estimation as compared to the estimation carried out by using longer wavelengths of about 10 μm. When, for example, 10% of the radiated energy from an object that has a temperature of about 800ºC is absorbed by the atmosphere, the estimated temperature decreases by about 100ºC when the 10 μm wavelength is used and by about 10ºC when the 1 μm wavelength is considered (Fig. 1).

Sensor

Most of the image sensors used in digital cameras are silicon devices such as CCD and CMOS. When photons come into the silicon sensor, the electrons in the silicon are excited and the covalent bonds that hold the electrons to the silicon atoms are broken. The number of electrons that are released increases with the intensity of light. Essentially, the energy of the photons has to be adequate to break the covalent bonds of the silicon in order to generate electrons (or electron-hole pairs). This requires that the energy of the photons be greater than the

energy gap of silicon (i.e., greater than about 1.1 eV). Generally, the light wavelengths in the visible spectrum and the near-infrared spectrum up to 1.1 μm have sufficient energy to liberate electrons. Silicon image sensors are thus sensitive to near-infrared wavelengths (Joyce, 1992; Theuwissen, 1995).

As mentioned previously, the radiation intensity in the near-infrared wavelengths is larger than the solar radiation for an object with a temperature higher than about 500ºC; the temperature resolution is higher and disturbances such as atmospheric absorption are expected to be smaller for the temperature estimation using the wavelengths. Therefore, a digital camera has an advantage with respect to monitoring the high-temperature areas in volcanoes.

In this study, a consumer digital camera Canon EOS 300D has been used whose price is less than $900. This camera has a six-megapixel CMOS-type image sensor and is widely used for astrophotography, where long-term exposures are common just to shoot a single scene, because of low noise and higher sensitivity in the near-infrared wavelengths. This camera is built on a professional single lens reflex (SLR) camera body, and the lens can be replaced. Further, the exposure time and the aperture value can be set to arbitrary values.

Consumer digital cameras using the silicon image sensors incorporate a band-pass filter, which transmits only the visible wavelengths. This filter has been removed in order to measure the intensity of light in the near-infrared spectrum.

Calibration

The sensitivity of image sensors used in consumer digital cameras is not generally open. In

this study, rock samples are heated in an electric furnace and the radiation of the rocks is recorded by the digital camera. The relation between the temperature of the samples and the recorded intensity of radiation is also obtained. In the Aso volcano, the active crater and its surrounding areas are covered with extrusive rocks of basaltic-andesite composition (Ono and Watanabe, 1985). In the measurements, rock samples collected at the rim of the active crater in the Aso volcano are used.

Radiance emitted from an object varies by several orders of magnitude within the temperature range as shown in Fig. 1. For the measurements, the exposure time and the aperture value are adjusted for obtaining an adequate amount of light on the image sensor after the sensitivity of the sensor S is set. The light value L, which is proportional to the intensity of the incident light in the lens, is calculated by using the exposure time t (s), the aperture value A (f-stop), and the sensitivity S (ISO) as follows:

$$L = L' A^2 / t / S,$$

where L' is the intensity of light recorded by the digital camera expressed as an 8-bit value in decimal. This value is plotted versus the object temperature in Fig. 2, in which a regression curve is also shown. From this figure, it is observed that the light value increases one order of magnitude with an increase in the temperature of 100ºC. This indicates that the error for the temperature estimation is less than a few tens of degrees, even if the light value varies by a factor of two. The lava samples used in the calibration are considered to have nearly the same emissivity values as basalt because their chemical composition is very close to that of basalt. The estimated emissivity value of basalt is about 0.95 as described above. The error in the

temperature estimation caused by the uncertainty of emissivity of 0.1 is less than 10ºC, and the emissivity value is not corrected in the calibration process.

Temperature estimation of a fumarole area in the active crater of the Aso volcano

Temperature measurements have been carried out at the Aso volcano located on the Kyushu island in the southwest Japan subduction zone (Fig. 3). This volcano is characterized by a very large caldera with the dimension of approximately 20 km, which was formed by an eruption of 90 ka. In this volcano, the strombolian eruptions occurred at intervals of 10 to 20 years, and the last one was in 1989; small phreatic eruptions occurred occasionally between the strombolian eruptions (Ono et al., 1995).

The active crater located in the Aso volcano is about 400 m in diameter. At the bottom of the active crater, there are a hot-water lake formed by the boiling springs and fumarole areas (Fig. 3). The temperatures of the hot-water lake and the fumaroles can be the indicator of magmatic activity; these temperatures increase before eruptions, which results in the dry-up of the lake and the glow of the fumaroles. Over one million tourists visit this volcano every year, and they can access to the edge of the active crater easily.

In this study, the temperature distribution of the fumarole area at the bottom of the active crater in the Aso volcano has been estimated by using a digital camera. The fumarole area is located at a distance of about 80 m below the crater edge. The camera is set at the crater edge, and the distance from the fumarole area to the camera is about 200 m. The images of the fumarole area are taken once a month from September to December in 2004. In the previous

measurement in November 2003, the temperature of the fumaroles in this area was estimated to be more than 800ºC by using a camcorder (Saito et al., 2005). Fumaroles with temperatures of about 800ºC can be seen clearly as bright spots in the images recorded in the previous measurements, unless they are in the sunlight. However, in September 2004, the fumaroles could not be identified in the recorded images taken in the daytime because of higher radiation noise from the surroundings, indicating a low temperature of the fumaroles. Thus, the images of the fumarole area were recorded during sunset in this study.

Results

An image of the fumarole area at the bottom of the active crater in the Aso volcano recorded in September 2004 is shown in Fig. 4(b). The width of this image area is about 30 m. In this image, the bright spots correspond to the fumaroles that cannot be seen as glowing spots with unassisted eyes, and the temperature of the fumaroles with a dimension of more than a few centimeters can be measured. The lens can be replaced easily, and the spatial resolution can be arbitrarily chosen. It can be seen from this image that the fumaroles with a diameter of less than 0.5 m are scattered in this fumarole area. The consumer camcorder used in the previous study was also used for the temperature measurement. An image recorded by the camcorder is shown in Fig. 4(c); the spatial resolution of this image is about four times smaller than that in Fig. 4(b). In this image, only one large bright spot can be identified, which corresponds to fumarole A shown in Fig. 4(b). The recorded image of this fumarole is blurred, but the temperature of the fumarole estimated from this image is nearly the same as that estimated by using the digital

camera.

The temperatures estimated for three of the brightest fumaroles shown in Fig. 4(b) are plotted in Fig. 5. The temperature estimated in November 2003 was over 800ºC, but the estimated temperatures were less than 500ºC in September and decreased over 50ºC from September to October; the temperatures showed a small decrease afterward. In March 2005, the radiation from the fumaroles could not be identified after sunset, indicating that the temperatures were less than about 300ºC.

Discussion

For the digital camera used in this study, the arbitrary values of A and t are chosen manually, and the intensity of the light at the sensor can be optimized to use the full range of the output signal from the sensor. The value of A and t were chosen automatically in the factory preset ranges and could not be varied manually for the camcorder. The camcorder probably chose the optimum values of A and t in the preset ranges, but the recorded light intensity was lower for the lower-temperature fumaroles. In Fig. 4(c), the maximum signal value is about 100 on a 256-scale intensity and the image of the bright spot becomes blurred, although clear images were recorded for higher-temperature fumaroles in the previous study (Saito et al., 2005).

In general, the depth of field increases as the aperture becomes smaller. For the camcorder, the aperture could not be set manually and probably became larger automatically for dark objects; the images recorded then blurred. In Fig. 4(c), the area of the small bright spots in Fig. 4(b) corresponds to that of several pixels. When the depth of field is small, it is difficult to focus

precisely at each of the small fumaroles and the image becomes blurred; the radiation energy from each of the small fumaroles is diffused in a larger area at the sensor, which results in the lower light intensity recorded in the camcorder. Then the other small bright spots shown in Fig. 4(b) cannot be detected in Fig. 4(c) due to the relatively low S/N ratio.

For the camcorder, the temperature, size, and distribution of the fumaroles could not be monitored accurately throughout the temperature range of the thermometer. For the digital camera, the depth of field and the light intensity at the sensor can be optimized manually by choosing the value of A and T, and the spatial resolution can be set by changing lenses. The fumarole activity can then be monitored reliably.

In Fig. 5, the temperature ranges measured in each month by the Japan Meteorological Agency (JMA) are also shown (JMA, 2004). The JMA measured the maximum temperature of the same fumarole area from the same camera position as the area considered in this study several times a month. The measured temperature by the JMA is about 200ºC lower than that estimated in this study; the temperature shows a decrease similar to that estimated in this study, but the temperature difference is smaller.

The temperatures measured by the JMA are considerably lower than those measured in this study. The JMA used a dedicated infrared thermometer that could measure temperatures lower than 500ºC, and the azimuthal resolution of the thermometer is 1° (Saito et al., 2005), which corresponds to the spatial resolution ~~is~~ of about 1 m in their measurements. The dimension of the fumaroles in this area is less than 1 m, and the lower spatial resolution as compared to the fumarole size may be the cause of the lower temperatures.

The atmospheric absorption can also be the cause of the difference of the measured temperatures. In active craters, the concentrations of water vapor, CO_2, and other gases from the fumaroles are probably higher, and the radiation energy absorbed through the atmosphere cannot be neglected. As mentioned previously, the temperature estimation using the wavelengths of about 10 μm is sensitive to the disturbances. In those wavelengths, the radiation intensity of an object with temperature of 400ºC differs from that of 200ºC by no more than one order of magnitude; the absorption of a few tens of percent of the radiation energy decreases the estimated temperatures by more than 100ºC. When the temperature difference of about 200ºC is caused only by the atmospheric absorption, 60% of the radiation energy is calculated to have been absorbed by the atmosphere in the wavelengths of 10 μm. In the wavelengths of 1 μm, this decrease in radiation intensity results in the error of the temperature estimation of only about 20ºC for a fumarole temperature of 400ºC. The decrease in the radiation intensity due to the atmospheric absorption can be estimated, when the temperature of an object in the crater is measured by using both the near- and the thermal-infrared wavelengths.

A decrease in the emissivity due to the alteration of rocks in the active crater may lower the radiation. When the emissivity of altered rocks is a half of that of fresh ones, the decrease in the estimated temperature is about 20ºC, as described for the atmospheric absorption. The error in the temperature estimation may be not more than 100ºC even for the high-temperature fumaroles in the active crater when the estimation is carried out by using the digital camera in the temperature range that the digital camera can measure. Further calibration would be useful especially for temperature measurements of various high-temperature bodies with higher

accuracy using the digital camera; temperature measurements of, for example, a body having smooth surfaces with known emissivity considering sunlight conditions can give reference light values for the temperature estimations.

Conclusions

In this study, a consumer digital camera is used as an infrared thermometer. The temperature distribution in the fumarole area in the active crater of the Aso volcano was estimated by using a digital camera. In the recorded images, small fumaroles were recognized clearly. For the digital camera, the values of A and t could be optimized manually and clear images could be obtained throughout the temperature range in which the digital camera could measure, while the images recorded by the camcorder became blurred for the low-temperature fumaroles. The digital camera measured the temperature by using shorter wavelengths, which was robust against atmospheric absorption and the other disturbances, and the estimated temperature was more reliable than that using the dedicated infrared thermometer used in the Aso volcano. The error in the estimated temperature of the fumaroles in the active crater was several times lower than that for the dedicated infrared thermometer. The temperature, size, and spatial distribution of fumaroles estimated by using the digital camera were considered to be more reliable than those obtained by the camcorder or the dedicated infrared thermometer. The consumer digital camera is handy and cost-effective, and has better temperature and spatial resolutions; this camera can be used for monitoring the high-temperature magmatic activity in volcanoes.

Acknowledgments:

I would like to thank K. Shibata, N. Murakami, S. Sasaki, H. Kobayashi, and K. Sawai for helping the temperature calibration of the digital camera infrared thermometer.

References

ASTM International, 2006. ACTIVE STANDARD: E490-00a(2006) Standard Solar Constant and Zero AIR MASS Solar Spectral Irradiance Tables. Book of Standards Volume, 15.03.

Baldridge, A.M., Hook, S.J., Grove, C.I. and Rivera, G., 2008. The ASTER spectral library version 2.0. Remote Sens. Environ., 113: 711-715.

Connor, C.B., Clement, B.M., Xiaodan, S., Lane, S.B. and West, T.J., 1993. Continuous monitoring of high-temperature fumaroles on an active lava dome, Volcan Colima, Mexico: evidence of mass flow variation in response to atmospheric forcing. Journal of Geophysical Research, 98: 19713-19722.

Flynn, L.P., Harris, A.J.L., Rotherly, D.A. and Oppenheimer, C., 2000. High-spatial-resolution thermal remote sensing of active volcanic features using Landsat and Hyperspectral data. In: P.J. Mouginis-Mark, J.A. Crisp and J.H. Fink (Editors), Remote Sensing of Active Volcanism. Geophysical Monograph. Am. Geophys. Union, Washington, D.C., pp. 161-177.

Giberti, G., Jaupart, C. and Sartoris, G., 1992. Steady-state operation of Stromboli volcano, Italy. Bulletine of Volcanology, 54: 535-541.

Harris, A.J.L. and Stevenson, D.S., 1997. Thermal observations of degassing open conduits and fumalores at Stromboli and Vulcano using remotely sensed data. Journal of Volcanology and Geothermal Research, 76: 175-198.

Japan Meteorological Agency, 2004. Annual Report on Volcanic Activity in Japan: Aso Volcano. pp. 19.

Joyce, R.R., 1992. Observing with infrared arrays. In: S.B. Howell (Editor), Astronomical CCD Observing and Reduction Techniques. Astron. Soc. Pac., San Francisco, pp. 258-284.

Martini, M., 1986. Thermal activity and ground deformation at Phlegrean Fields, Italy: precursors of eruptions or fluctuations of quiescent volcanism? A contribution of geochemical studies. Journal of Geophysical Research, 91: 12255-12260.

Menyailov, I.A., Nikitina, L.P., Shapar, V.N. and Pilipenko, V.P., 1986. Temperature increase and chemical change of fumaloric gases at Momotombo volcano, Nicaragua, in 1982-1985: are these indicators of a possible eruption? Journal of Geophysical Research, 91: 12199-12214.

Ono, K. and Watanabe, K., 1985. Geological map of Aso volcano, Geological Map of Volcanoes. Geol. Surv. Japan.

Ono, K., Watanabe, K., Hoshizumi, H. and Ikebe, S., 1995. Ash eruption of the Naka-dake crater, Aso volcano, southwestern Japan. Journal of Volcanology and Geothermal Research, 66: 137-148.

Ramsey, M. and Dehn, J., 2004. Spaceborne observations of the 2000 Bezymianny, Kamchatka eruption: the integration of high-resolution ASTER data into near real-time monitoring using AVHRR. Journal of Volcanology and Geothermal Research, 135: 127-146.

Ripepe, M., Harris, A.J.L. and Carniel, R., 2002. Thermal, seismic and infrasonic evidences of variable degassing rates at Stromboli volcano. Journal of Volcanology and Geothermal Research, 118: 285-297.

Saito, T. et al., 2005. A new technique of radiation thermometry using a consumer digital camcorder: Observations of red glow at Aso volcano, Japan. Earth Planets Space, 57: e5-e8.

Salisbury, J.W. and D'Aria, D.M., 1994. Emissivity of terrestrial materials in the 3-5 μm atmospheric window. Remote Sensing of Environment, 47: 345-361.

Stevenson, D.S., 1993. Physical models of fumaloric flow. Journal of Volcanology and Geothermal Research, 57: 139-156.

Taran, Y.A., Hedenquist, J.W., Korzhinsky, M.A., Tkachenko, S.I. and Shmulovich, K.I., 1995. Geochemistry of magmatic gases from Kudriavy volcano, Kuril Islands. Geochimica Cosmochimica Acta, 59: 1749-1761.

Theuwissen, A.J.P., 1995. Solid-State Imaging with Charge-Coupled Devices. Kluwer Academic Publishers, Dordrecht/Boston/London.

Figure captions

Fig. 1 Black-body radiance is plotted with the wavelength. The numbers denote temperature (K). Solar radiation at the surface is also shown (ASTM International, 2006).

Fig. 2 Measured radiation intensity from a rock sample heated in an electric furnace at temperatures up to 900ºC.

Fig. 3 Topographic map of the active crater of the Aso volcano. The crater rim is denoted by the thick line. The hatched circle and the triangle represent the fumarole area and the observation point, respectively. The inset denotes the location of the Aso volcano.

Fig. 4 Photographs of the fumarole area at the bottom of the active crater in the Aso volcano. (a) Daytime photo taken by a normal camera; (b) image recorded by the infrared digital camera (f = 300 mm, f-stop = 5.6, t = 2 sec., ISO = 800). Temperature was estimated in three fumaroles (A, B, and C) in this figure; and (c) image recorded by the camcorder. The blurred light spot in the center of the image is the fumarole A in the middle image. The circle indicates the same area as that in the middle figure.

Fig. 5 Estimated temperatures of the three fumaroles shown in Fig. 4(b). The hatched rectangles denote the monthly variation in peak temperatures in the fumarole area measured several times a month by the Japan Meteorological Agency (JMA, 2004).

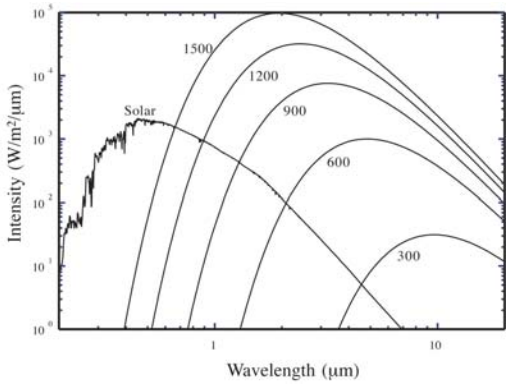

Fig. 1

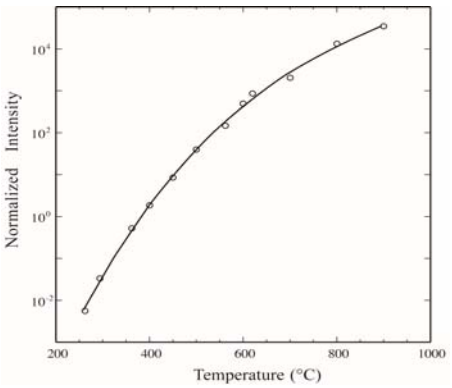
Normalized Intensity
10^{4}
10^{2}
10^{0}
10^{-2}
200
400
600
800
1000
Temperature (°C)

Fig. 2

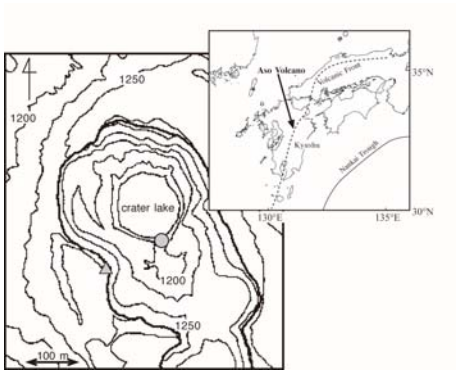
1250
1200
crater lake
1200
1250
100 m
Aso Volcano
Median Tect
Kyushu
Nankai Trough
35°N
30°N
130°E
135°E

Fig. 3

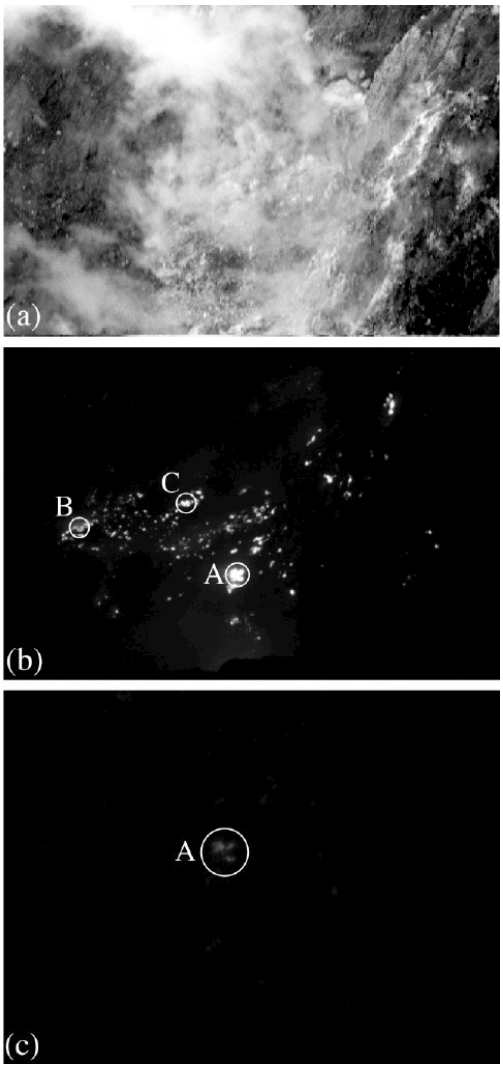

Fig. 4

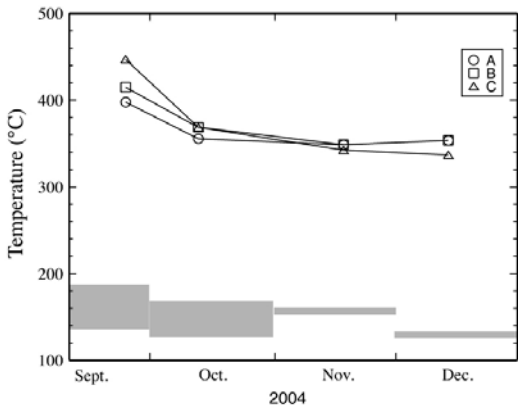

Fig. 5